ACS OMEGA

http://pubs.acs.org/journal/acsodf

Article

# Polyacrylic Acid-Functionalized Graphene@$Ca(OH)_2$ Nanocomposites for Mural Protection

Wenting Gu,[§] Yanfei Wei,[§] Bingbing Liu, Liuyong Hu, Lei Zhong, and Guoke Chen*

Cite This: *ACS Omega* 2022, 7, 12424−12429

Read Online

ACCESS | Metrics & More | Article Recommendations | Supporting Information

**ABSTRACT:** Murals are one of the precious legacies of our ancestors; however, they face severe damage along with archeological discoveries, which need urgent repair. Nowadays, nanotechnology provides new concepts and materials for the consolidation and protection of murals. In this work, an innovative method for the protection of murals was proposed with graphene-based nanomaterials through strategically synthesizing a polyacrylic acid-functionalized graphene/nano-$Ca(OH)_2$ material (PAAG@$Ca(OH)_2$) by a facile and economic aqueous method. As a result, the nanocomposite PAAG@$Ca(OH)_2$ was demonstrated with high porosity, strong adsorption, appropriate hydrophilicity, and better permeability compared to the commercial AC33 sample according to the simulated tests. As expected, the nanocomposite PAAG@$Ca(OH)_2$ displayed a promising application for the reinforcement of murals, which opens up a new avenue for the protection of murals.

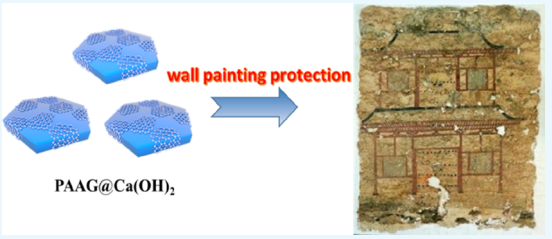


## 1. INTRODUCTION

Murals are an important part of humankind's excellent cultural heritage.[1] However, murals always face severe damage over the years, such as flaking (Figure 1A,B), hollowing (Figure 1C), fungus damage, and cracks. Therefore, the development of mural reinforcement materials becomes more and more indispensable for the protection of cultural heritage.[2,3] In the past decades, the diagnosis and conservation of cultural heritage have attracted broad attention in the field of materials science.[4] The reinforcement materials of murals are mainly divided into inorganic materials and organic materials. Inorganic materials mainly involve lime water, barium hydroxide, and alkaline earth silicate. In the early days, Dutkiewicz used lime water to reinforce the frescoes of Russian churches.[5] Subsequently, barium hydroxide has been applied gradually in the field of mural or stone reinforcement. However, the usage of inorganic materials will inevitably carry the aqueous solution into the mural, which will result in the crystallization of soluble salts.[6] Meanwhile, the large size of inorganic materials leads to poor permeability, which will limit the strength of mural reinforcement. Recently, owing to excellent permeation, good adhesion, and transparency, organic acrylic polymers have been applied to the reinforcement of murals, such as Paraloid B-72 and Primal AC33.[7] However, an organic polymer material exhibits an obvious aging problem after thermal oxidation and optical irradiation, which induces the degradation of mechanical strength. When the Cholula murals in Mexico were reinforced with polyvinyl acetate and Paraloid B-72, the paint layer had fallen away from the ground layer after being restored for about 20 years, resulting from the crystallization of soluble salts on the surface. The main reason is that the polymer blocks the surface pores and hinders the interaction between the mural and the environment, which generates mechanical stresses in the mural layer.

In recent years, with the rise of various nanomaterials, their unique nanoparticle size and physicochemical properties have attracted attention in the field of heritage protection.[8−16] For example, Giorgi et al. carried out research on nanocalcium hydroxide in the mural restoration of Mexican murals and the La Antigua Ciudad Maya de Calakmul World Cultural Heritage Site.[17] Nevertheless, low mechanical strength and carbonization still exist in the murals. Since graphene has made giant progress in experiment, a lot of attention has been focused on the application of graphene due to its unique structure of a single planar sheet of $sp^2$-bonded carbon atoms, which endows it with excellent physical and chemical properties, such as a high surface area and excellent electrical and thermal properties.[18−22] Graphene has been widely applied in the fields of optical electrodes, optoelectronic devices, sensors, and photocatalysis.[23−26] To date, graphene has been less studied in the field of heritage protection, particularly in the consolidation materials for murals.

In this work, we integrated polyacrylic acid-functionalized graphene with nano-$Ca(OH)_2$ (PAAG@$Ca(OH)_2$) for better protection of murals. Benefiting from the large specific surface

Received: March 7, 2022
Accepted: March 24, 2022
Published: April 3, 2022

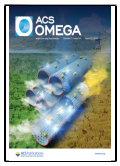





https://doi.org/10.1021/acsomega.2c01364
*ACS Omega* 2022, 7, 12424−12429

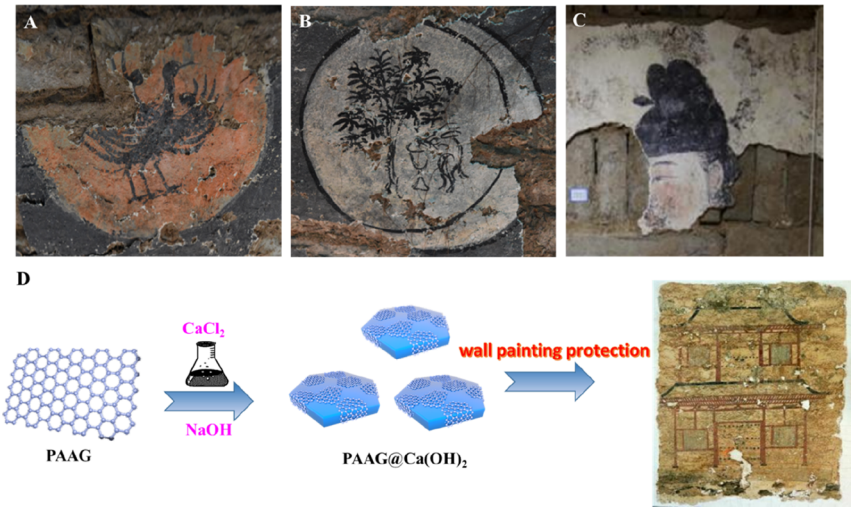


**Figure 1.** Digital pictures of murals from the Murongzhi tomb of the Tang dynasty with the problems of flaking on the painting surface (A,B) and hollowing phenomena (C). Synthetic method of PAAG@$Ca(OH)_2$ nanocomposites (D).

area of graphene, the fabricated PAAG@$Ca(OH)_2$ can easily capture and store $CO_2$ under the ambient environment. In addition, the as-prepared nanocomposite PAAG@$Ca(OH)_2$ possesses high porosity, strong adsorption, appropriate hydrophilicity, and better permeability compared with the commercial AC33 through the simulated tests. As a result, the PAAG@$Ca(OH)_2$ exhibits a potential application for the reinforcement of murals.

## 2. EXPERIMENTAL SECTION

**2.1. Chemicals and Reagents.** Polyacrylic acid (PAA) ($M_w$ = 25,000) was purchased from Aldrich (St. Louis, USA). Graphite powder was bought from Alfa Aesar. Sodium hydroxide (NaOH) and calcium chloride dihydrate ($CaCl_2 \cdot 2H_2O$) were obtained from Beijing Chemical Reagent. The aqueous solutions were prepared with Millipore Milli-Q (18.2 MΩ cm) deionized water.

**2.2. Apparatuses.** The transmission electron microscopy (TEM) image, high-resolution transmission electron microscopy (HRTEM) image, high-angle annular dark-field−scanning transmission electron microscopy (HAADF−STEM) image, selected-area electron diffraction (SAED) pattern, energy-dispersive X-ray (EDX) spectra, and elemental mapping images were tested by a TECNAI G2 high-resolution transmission electron microscope (Hitachi, Tokyo, Japan) with an accelerating voltage of 200 kV. Scanning electron microscope (SEM) images were recorded with an XL30 ESEM FEG SEM (Philips, The Netherlands) operating with an accelerating voltage of 20 kV. X-ray photoelectron spectroscopy (XPS) analysis was recorded with an ESCALAB-MKII X-ray photoelectron spectrometer (VG Scientific, UK). Powder X-ray diffraction (XRD) patterns were obtained from a D8 ADVANCE diffractometer (Germany) using Cu K$\alpha$ radiation ($\lambda$ = 1.5406 Å).

**2.3. Synthesis of Polyacrylic Acid-Functionalized Reduced Graphene Oxide (PAAG).** For the synthesis of graphene oxide (GO), graphite oxides were obtained from natural graphite powder by the Hummers method.[27] To exfoliate the graphite oxide into graphene oxide, the sample was processed under ultrasonication for 60 min (1000 W, 27% amplitude) and centrifugation at 5000 rpm for 30 min. Finally, a homogeneous graphene oxide (GO) dispersion with a concentration of 0.4 mg $mL^{-1}$ was prepared.

For the preparation of polyacrylic acid-functionalized reduced graphene oxide (PAAG), 172 mg of polyacrylic acid (PAA) was added into 40 mL of the as-prepared exfoliated GO dispersion (0.4 mg $mL^{-1}$) and then stirred for 20 min. After stirring for 2 h at 90 °C, the resulting stable black mixture was centrifuged at 15,000 rpm and washed with DI water five times to remove the excess polymer.

**2.4. Preparation of the PAAG@$Ca(OH)_2$ Samples.** PAAG (30 mg) and 3.0 g of NaOH were dissolved in 100 mL of DI water. At the same time, 13.23 g of $CaCl_2 \cdot 2H_2O$ was also dissolved in 100 mL of DI water. Then, the two solutions were both heated to 90 °C and mixed quickly. When the solution was cooled to room temperature, the product PAAG@$Ca(OH)_2$ was obtained and washed with DI water five times to remove the impurity adsorbed on the surface of the product.

**2.5. Preparation of Simulated Samples.** The plaster layer of simulated wall painting samples was mainly wet slaked lime, and the hemp fibers were in a silicone mold having a volume of 10 × 10 × 1 $cm^3$. A small amount of short hemp fibers was added into the wet slaked lime in order to ease the shrinkage of the plaster layer during drying. All the samples were then left in an ambient room for a month to reach carbonation before further tests. The pigments were painted after the carbonation of the samples, and the pigments used here were cinnabar (red), ultramarine (blue), yellow ochre (yellow), and malachite (green).

## 3. RESULTS AND DISCUSSION

**3.1. Characterization of PAAG@$Ca(OH)_2$ Nanocomposites.** As shown in Figure 1D, the PAAG@$Ca(OH)_2$ nanocomposites were fabricated by an economical and facile method. Initially, PAAG was fabricated by a hydrothermal method (see Section 2.3) followed by mixing of the $CaCl_2$ solution, which contained a certain amount of NaOH at an elevated temperature. Then, the PAAG@$Ca(OH)_2$ nanocomposites were obtained after washing several times with DI water. Figure 2A shows the TEM image of the PAAG@$Ca(OH)_2$ nanocomposites, and the afforded PAAG@$Ca(OH)_2$ exhibits a hollow nanostructure, which is beneficial to


https://doi.org/10.1021/acsomega.2c01364
ACS Omega 2022, 7, 12424−12429

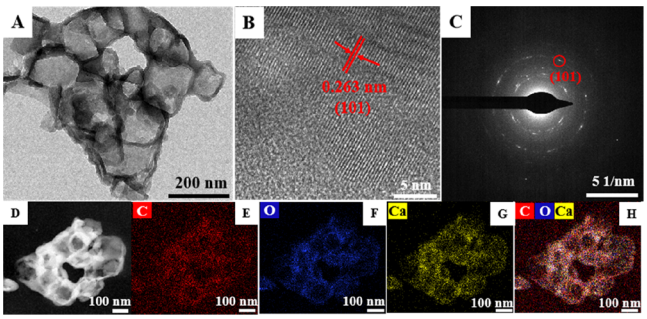


**Figure 2.** TEM image (A), HRTEM image (B), SAED pattern (C), HAADF−STEM image (D), and elemental mapping images (E−H) of PAAG@$Ca(OH)_2$.

mural protection. Moreover, the HRTEM image (Figure 2B) was investigated to better understand the PAAG@$Ca(OH)_2$ nanocomposites. The lattice distance of 0.263 nm should be assigned to the (101) crystal plane of the $Ca(OH)_2$ phase, which is consistent with the SAED pattern of the nanocomposites (Figure 2C). Figure 2D−H shows the HAADF−STEM and the elemental mapping images of the PAAG@$Ca(OH)_2$ nanocomposites. It could be observed that C, O, and Ca elements were evenly distributed over the selected area, implying a good mixture of PAAG and $Ca(OH)_2$. The morphologies of fabricated PAAG@$Ca(OH)_2$ nanocomposites were also studied with SEM. As shown in Figures S1 and S2, the $Ca(OH)_2$ nanoparticles were uniformly distributed on the PAAG surface at different magnifications. EDX spectroscopy (Figure S3) was also conducted to measure the elemental contents of the prepared PAAG@$Ca(OH)_2$ nanocomposite, which is made up of C (35.25 at. %), O (47.13 at. %), and Ca (17.62 at. %).

XRD measurements were used to understand the crystal structure of the obtained PAAG@$Ca(OH)_2$ nanocomposites. As observed in Figure 3A, the presence of the peaks located at 18.05, 28.60, 33.94, 46.97, 50.71, 54.28, 59.30, 62.56, 64.24, 71.85, and 84.59° correspond to the (001), (100), (101), (102), (110), (111), (200), (201), (103), (202), and (104) planes of $Ca(OH)_2$ (JCPDS file no. 441481), respectively.

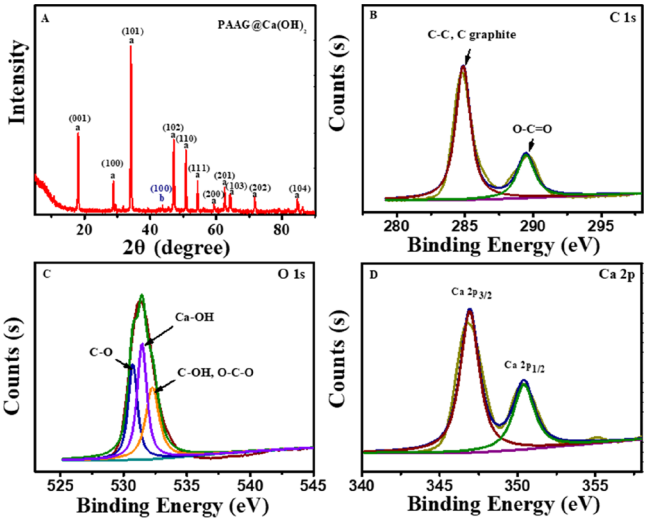


**Figure 3.** XRD pattern of PAAG@$Ca(OH)_2$ (A). High-resolution C 1s XPS spectra (B), O 1s spectra (C), and Ca 2p spectra (D) of the PAAG@$Ca(OH)_2$.

Meanwhile, the peak at around 43.60° corresponds to the (100) plane of the PAAG, suggesting that PAAG@$Ca(OH)_2$ nanocomposites were successfully prepared.

XPS tests were conducted to understand the chemical state of the elements in the PAAG@$Ca(OH)_2$ nanocomposites. As shown in Figure S4, the three elements C, O, and Ca were observed in the XPS survey spectra of PAAG@$Ca(OH)_2$. Figure 3B shows the C 1s XPS spectra of PAAG@$Ca(OH)_2$ with the peaks located at 284.8 and 289.48 eV, which should correspond to the C−C group along with the O−C═O group, indicating the carbon elemental environments of PAAG@$Ca(OH)_2$ nanocomposites. Moreover, the peaks located at 530.69, 531.49, and 532.28 eV in the high-resolution O 1s XPS spectra (Figure 3C) were assigned to the C−O, Ca−O, and C−OH/O−C−O groups, respectively. The Ca 2p spectrum exhibited in Figure 3D could be divided into two peaks (346.92 and 350.41 eV), which were related to the $2p_{3/2}$ of $Ca^{2+}$ and $2p_{1/2}$ of $Ca^{2+}$, which indicates the presence of $Ca(OH)_2$ crystals in the PAAG@$Ca(OH)_2$ nanocomposites and further implies the successful preparation of the PAAG@$Ca(OH)_2$ nanocomposites.

**3.2. Reinforcement Efficiency of PAAG@$Ca(OH)_2$ Nanocomposites for Murals.** In order to evaluate the reinforcement efficiency of the PAAG@$Ca(OH)_2$ nanocomposite for murals, we first carried out a test with the simulated murals. Specifically, a 5 mg/mL PAAG@$Ca(OH)_2$ nanocomposite was dissolved in ethanol and then brushed on the surface of the mural simulated sample until it cannot penetrate. Afterward, the sample blocks were placed in a constant-temperature humidity chamber with an open hole diameter of 50 mm for 15 days to allow carbon dioxide to carbonize calcium hydroxide in PAAG@$Ca(OH)_2$. The temperature and humidity were set to 25 °C and 65%, respectively. For comparison, the commercial AC33 was used as a reference material. In general, the color change is an important factor to evaluate the rationality of the reinforcement material.[28] Based on the chromatic aberration measurement, the effect of PAAG@$Ca(OH)_2$ and AC33 on the mural has been evaluated. By contrasting the color changes after reinforcement, the chromatic aberration $\Delta E$ was calculated as follows:

$$\Delta E = \sqrt{\Delta L^2 + \Delta a^2 + \Delta b^2}$$

where $L$ represents illuminance, which is equivalent to brightness. $a$ represents the range from magenta to green, and $b$ represents the range from yellow to blue. $\Delta L$, $\Delta a$, and $\Delta b$ are the differences of $L$, $a$, and $b$ before and after the measurement, respectively.

As shown in Table 1, the $L$, $a$, and $b$ of the standard sample are $L$ = 96.12, $a$ = 0.33, and $b$ = 2.66, respectively. We selected three points to measure the $L$, $a$, and $b$ values before and after

**Table 1. The Change of Color after Mural Reinforcement by AC33 and PAAG@$Ca(OH)_2$**

| sample type | $\Delta L$ | $\Delta a$ | $\Delta b$ | $\Delta E$ |
|---|---|---|---|---|
| AC33 | −6.20 | −0.97 | 1.13 | 6.38 |
| | −5.41 | −1.21 | 1.02 | 5.64 |
| | −6.19 | −1.67 | 0.97 | 6.48 |
| PAAG@$Ca(OH)_2$ | −2.37 | 1.00 | 3.37 | 4.24 |
| | −1.25 | 0.96 | 2.15 | 2.67 |
| | −1.56 | 1.13 | 2.43 | 3.10 |



https://doi.org/10.1021/acsomega.2c01364
ACS Omega 2022, 7, 12424−12429

the reinforcement of PAAG@Ca(OH)$_2$ and AC33. The calculation shows that the $\Delta E$ values of PAAG@Ca(OH)$_2$ are less than 5 (Table 1), while the $\Delta E$ values of AC33 are larger than 5. Therefore, the color of simulated samples had no significant changes after being reinforced with PAAG@Ca(OH)$_2$, which demonstrates that PAAG@Ca(OH)$_2$ has less effect on the color of the mural.

As far as we know, the porosity test is another important means to evaluate the reinforcement performance for murals. A mercury porosimeter was used to measure the pore size distribution and porosity. In Figure 4, the pore size of the mural sample was distributed over 0−2000 nm, and the pore size diameter was mainly located at about 1000 nm. The porosity of the untreated sample was 53.64%. As shown in Table S1, the porosity has a slight reduction after reinforcement by AC33 (53.2182%), while the porosity has a slight increase after reinforcement by PAAG@Ca(OH)$_2$ (54.10%). These results indicate that the internal structure of the mural will not change greatly after the reinforcement with PAAG@Ca(OH)$_2$. Therefore, it can be inferred that PAAG@Ca(OH)$_2$ is an excellent material for the reinforcement of murals.

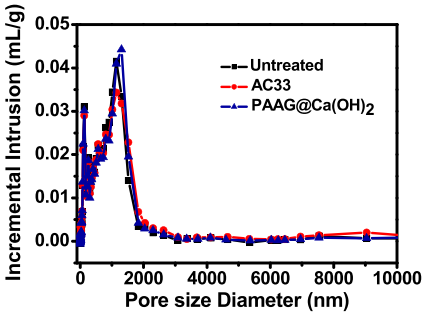


**Figure 4.** Aperture dimensions of the untreated samples and those consolidated by the as-prepared AC33 and PAAG@Ca(OH)$_2$.

**3.3. The Bonding Strength of PAAG@Ca(OH)$_2$ Nanocomposites for Murals.** The "Scotch tape test" (STT) was also performed to evaluate the bonding strength of the PAAG@Ca(OH)$_2$. The weight loss taken up by the Scotch tape is shown in Figure 5A,B. For the untreated sample, which was not coated with any reinforcing material, the weight loss is 3.21 ± 0.5 mg cm$^{-2}$. The weight loss of the simulated samples consolidated with the AC33 is 1.54 ± 0.5 mg cm$^{-2}$. However, the weight loss is only 0.71 ± 0.3 mg cm$^{-2}$ for the simulated samples consolidated with the PAAG@Ca(OH)$_2$ nanohybrids, which also proves that PAAG@Ca(OH)$_2$ is an effective consolidation material for murals. The carbonation process transforming Ca(OH)$_2$ to CaCO$_3$ is the crucial reason for the better STT result.[29−31] It is well-known that graphene has a large specific surface area, which can constantly capture, store, and release CO$_2$ to adjacent Ca(OH)$_2$.[32] Thus, the fabricated PAAG@Ca(OH)$_2$ could easily capture and store CO$_2$ even under an ambient environment. Furthermore, the mural samples reinforced with AC33 and PAAG@Ca(OH)$_2$ were also tested by SEM. It can be seen from Figure S5A that the untreated mural sample was porous and loose, which is consistent with the porosity and strength tests. After being reinforced with AC33 and PAAG@Ca(OH)$_2$, the mural samples became compact (Figure S5B,C). In particular, after the sample block was reinforced by PAAG@Ca(OH)$_2$, the apparent cavity almost disappeared. The results further reveal that the strength of murals can be improved by PAAG@Ca(OH)$_2$.

**3.4. The Hydrophilicity of PAAG@Ca(OH)$_2$ Nanocomposites for Murals.** The exchange of moisture has an important impact on the mural pigment between air and the base layer. Therefore, it is important to explore the hydrophilic performance of different consolidated materials. It is mainly hydrophilic when the contact angle is less than 90° on the surface of the mural. Compared with the untreated samples (Figure 5C), the hydrophobicity was increased slightly after reinforcement with AC33 (Figure 5D) and PAAG@Ca(OH)$_2$ (Figure 5E). The hydrophobicity change is not significant. So, PAAG@Ca(OH)$_2$ has less effect of moisture exchange on the mural, which can be used to strengthen the pigment layer of the mural.

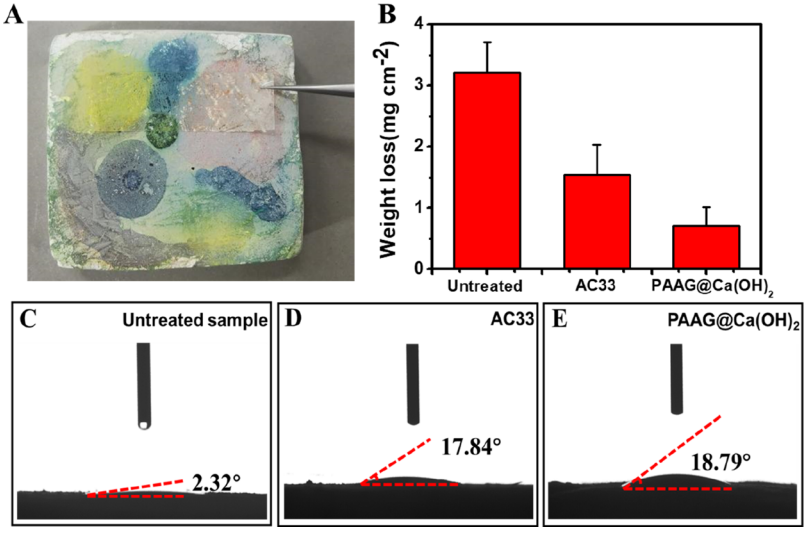


**Figure 5.** Digital picture of the "Scotch tape test" (STT) (A) and weight loss of the simulated murals (B) with the untreated samples and consolidated with the as-prepared AC33 and PAAG@Ca(OH)$_2$ materials (the untreated samples denote that the samples were not treated with any consolidation material); contact angles of the different materials, namely, the untreated sample (C) and the as-prepared AC33 (D) and PAAG@Ca(OH)$_2$ (E) consolidated murals.



https://doi.org/10.1021/acsomega.2c01364
ACS Omega 2022, 7, 12424−12429

**3.5. The Permeability of PAAG@Ca(OH)$_2$ Nanocomposites for Murals.** Permeability also plays a significant role in mural consolidation.[27] The penetration depth can be compared based on the Raman spectral test of AC33 and PAAG@Ca(OH)$_2$ consolidated murals. As shown in Figure 6A, the D and G bands are attributed to graphene in the

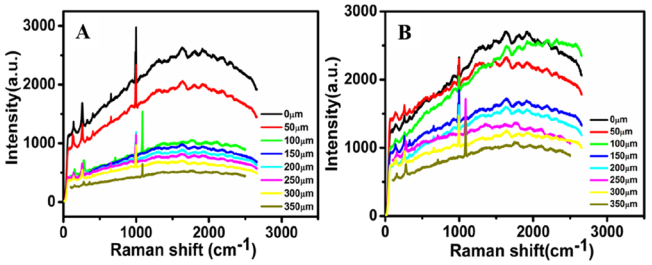


**Figure 6.** Raman spectra of the as-prepared AC33 (A) and PAAG@Ca(OH)$_2$ (B) consolidated mural cross sections at different depths.

PAAG@Ca(OH)$_2$. Therefore, the shifts from the surface to the location of the D and G of PAAG@Ca(OH)$_2$ are not detectable along the depth of penetration. For the as-prepared AC33 consolidated mural sample, the Raman peaks of the AC33 (Figure 6B) were around 1457 and 1683 cm$^{-1}$, and the intensity appeared from 0 to 200 $\mu$m and decreased from 200 to 350 $\mu$m, demonstrating that the penetration depth was about 200 $\mu$m. Meanwhile, for the PAAG@Ca(OH)$_2$ consolidated mural sample, the intensity of the D band and the G band gradually decreased from 0 to 300 $\mu$m. At 350 $\mu$m, the intensity of the two bands can be negligible, which means that the penetration depth is about 350 $\mu$m. The results show that the PAAG@Ca(OH)$_2$ nanocomposite can permeate much deeper in the mural than AC33, which demonstrates an important application of PAAG@Ca(OH)$_2$ as a promising material for murals.

## 4. CONCLUSIONS

In this work, we demonstrate an unprecedented concept of mural protection enabled by polyacrylic acid-functionalized graphene through strategically synthesizing nanocomposites (PAAG@Ca(OH)$_2$) using a facile and economic aqueous method. Through the simulated mural, the PAAG@Ca(OH)$_2$ nanocomposite displays high porosity, strong adsorption, appropriate hydrophilicity, good permeability, and strong adhesion to mural pigments, which is a potential candidate to consolidate murals. As a result, the PAAG@Ca(OH)$_2$ nanocomposite shows superior conservation efficiency to the AC33, which demonstrates an important application of graphene as a protective material for reinforcement of murals.

## ■ ASSOCIATED CONTENT

### Supporting Information

The Supporting Information is available free of charge at https://pubs.acs.org/doi/10.1021/acsomega.2c01364.

SEM images of PAAG (Figure S1) and PAAG@Ca(OH)$_2$ (Figure S2); EDX image of PAAG@Ca(OH)$_2$ (Figure S3); XPS survey spectrum of PAAG@Ca(OH)$_2$ (Figure S4); SEM images of untreated samples and the as-prepared AC33 and PAAG@Ca(OH)$_2$ consolidated wall paintings (Figure S5); porosity of the untreated samples and those consolidated by as-prepared AC33 and PAAG@Ca(OH)$_2$ (Table S1) (PDF)

## ■ AUTHOR INFORMATION


### Corresponding Author

**Guoke Chen** − *Institute of Cultural Relics and Archaeology of Gansu, Lanzhou 730000, P. R. China*; Email: chenguoke1980@sina.com

### Authors

**Wenting Gu** − *Institute of Cultural Relics and Archaeology of Gansu, Lanzhou 730000, P. R. China*; orcid.org/0000-0003-2980-1795

**Yanfei Wei** − *Institute of Cultural Relics and Archaeology of Gansu, Lanzhou 730000, P. R. China*

**Bingbing Liu** − *Institute of Cultural Relics and Archaeology of Gansu, Lanzhou 730000, P. R. China*

**Liuyong Hu** − *Hubei Key Laboratory of Plasma Chemistry and Advanced Materials, Hubei Engineering Technology Research Center of Optoelectronic and New Energy Materials, Wuhan Institute of Technology, Wuhan 430205, P. R. China*

**Lei Zhong** − *Institute of Cultural Relics and Archaeology of Gansu, Lanzhou 730000, P. R. China*

Complete contact information is available at: https://pubs.acs.org/10.1021/acsomega.2c01364

### Author Contributions

[§]W.G. and Y.W. contributed equally to the article.


### Author Contributions

W.G. designed the experiments, prepared the samples, performed the data analysis, and wrote the manuscript. B.L. provided the photographs and wrote and revised the article. Y.W. helped in writing and revising the article. L.H. performed the experiment and analyzed the data. L.Z. performed the experiments. G.C. wrote and revised the article.

### Notes

The authors declare no competing financial interest.

## ■ ACKNOWLEDGMENTS

This work was financially supported by the National Social Science Fund Key Project of Research on the Unearthed Data from the Tomb of Murongzhi (Xiwang) (project number 20AKG007), the National Cultural Heritage Administration Project of Archaeological China-Archaeology of the Tuyuhun Tombs of the Tang Dynasty, and the Gansu Provincial Cultural Relics Protection Science and Technology Research project of Application Research of Polyacrylic Acid-Functionalized Graphene/Nano-Ca(OH)$_2$ in Mural Reinforcement.

## ■ REFERENCES

(1) Giorgi, R.; Baglioni, M.; Berti, D.; Baglioni, P. New Methodologies for the Conservation of Cultural Heritage: Micellar Solutions, Microemulsions, and Hydroxide Nanoparticles. *Acc. Chem. Res.* **2010**, *43*, 695−704.

(2) Baglioni, P.; Chelazzi, D.; Giorgi, R. Nanomaterials in art conservation. *Nat. Nanotechnol.* **2015**, *10*, 287.

(3) Jroundi, F.; Schiro, M.; Ruiz-Agudo, E.; Elert, K.; Martin-Sanchez, I.; Gonzalez-Munoz, M. T.; Rodriguez-Navarro, C. Protection and Consolidation of Stone Heritage by Self-Inoculation with Indigenous Carbonatogenic Bacterial Communities. *Nat. Commun.* **2017**, *8*, 279.

(4) Baglioni, M.; Poggi, G.; Chelazzi, D.; Baglioni, P. Advanced Materials in Cultural Heritage Conservation. *Molecules* **2021**, *26*, 3967.

(5) Dutkiewicz, J. E. The discovery and conservation of 14 - 16th century wall - paintings in the presbytery of the church in Olkusz. *Ochrona Zabytkow* **1964**, 11−35.
(6) Wang, Z.; Su, B.-m.; Yu, Z.-r.; Shui, B.-w.; Zhao, J.-l.; Cui, Q.; Shan, Z.-w.; Li, Q. In-Situ Non-Invasive FTIR Analysis of Conservation Materials on the Surface of Mural Paintings in Prince Shi' s Palace of the Taiping Heavenly Kingdom. *Spectrosc. Spectral Anal.* **2020**, *40*, 356−361.
(7) Horie, V. *Acrylic polymers, Materials for Conservation: Organic Consolidants, Adhesives and Coatings*; Butterworth-Heinemann: Oxford, 2010, pp.153−172.
(8) Poggi, G.; Giorgi, R.; Mirabile, A.; Xing, H.; Baglioni, P. A Stabilizer-Free Non-Polar Dispersion for the Deacidification of Contemporary Art on Paper. *J. Cult. Heritage* **2017**, *26*, 44.
(9) Poggi, G.; Toccafondi, N.; Chelazzi, D.; Canton, P.; Giorgi, R.; Baglioni, P. Hydroxide Nanoparticles for Cultural Heritage: Consolidation and Protection of Wall Paintings and Carbonate Materials. *J. Colloid Interface Sci.* **2016**, *473*, 42−49.
(10) Rodriguez-Navarro, C.; Ruiz-Agudo, E. *Pure Appl. Chem.* **2017**, *90*, 523.
(11) Chelazzi, D.; Poggi, G.; Jaidar, Y.; Toccafondi, N.; Giorgi, R.; Baglioni, P. *J. Colloid Interface Sci.* **2013**, *392*, 42.
(12) Cavallaro, G.; Milioto, S.; Parisi, F.; Lazzara, G. Halloysite Nanotubes Loaded with Calcium Hydroxide: Alkaline Fillers for the Deacidification of Waterlogged Archeological Woods. *ACS Appl. Mater. Interfaces* **2018**, *10*, 27355−27364.
(13) Giorgi, R.; Chelazzi, D.; Baglioni, P. Nanoparticles of Calcium Hydroxide for Wood Conservation. The Deacidification of the Vasa Warship. *Langmuir* **2005**, *21*, 10743−10748.
(14) Cavallaro, G.; Danilushkina, A.; Evtugyn, V.; Lazzara, G.; Milioto, S.; Parisi, F.; Rozhina, E.; Fakhrullin, R. Halloysite Nanotubes: Controlled Access and Release by Smart Gates. *Nanomaterials* **2017**, *7*, 199.
(15) Poggi, G.; Toccafondi, N.; Melita, L. N.; Knowles, J. C.; Bozec, L.; Giorgi, R.; Baglioni, P. Calcium Hydroxide Nanoparticles for the Conservation of Cultural Heritage: New Formulations for the Deacidification of Cellulose-Based Artifacts. *Appl. Phys. A: Mater. Sci. Process.* **2014**, *114*, 685−693.
(16) Caruso, M. R.; Megna, B.; Lisuzzo, L.; Cavallaro, G.; Milioto, S.; Lazzara, G. Halloysite Nanotubes-Based Nanocomposites for the Hydrophobization of Hydraulic Mortar. *J. Coat. Technol. Res.* **2021**, *18*, 1625−1634.
(17) Giorgi, R.; Ambrosi, M.; Toccafondi, N.; Baglioni, P. Nanoparticles for Cultural Heritage Conservation: Calcium and Barium Hydroxide Nanoparticles for Wall Painting Consolidation. *Chem. − Eur. J.* **2010**, *16*, 9374.
(18) Li, X.; Choy, W. C. H.; Ren, X.; Zhang, D.; Lu, H. Highly Intensified Surface Enhanced Raman Scattering by Using Monolayer Graphene as the Nanospacer of Metal Film-Metal Nanoparticle Coupling System. *Adv. Funct. Mater.* **2014**, *24*, 3114.
(19) Li, X.; Tong, T.; Wu, Q.; Guo, S.; Song, Q.; Han, J.; Huang, Z. Unique Seamlessly Bonded CNT@Graphene Hybrid Nanostructure Introduced in an Interlayer for Efficient and Stable Perovskite Solar Cells. *Adv. Funct. Mater.* **2018**, *28*, No. 1800475.
(20) Guo, S.; Li, X.; Ren, X.; Yang, L.; Zhu, J.; Wei, B. Optical and Electrical Enhancement of Hydrogen Evolution by $MoS_2$@$MoO_3$ Core-Shell Nanowires with Designed Tunable Plasmon Resonance. *Adv. Funct. Mater.* **2018**, *28*, No. 1802567.
(21) Song, Q.; Ye, F.; Yin, X.; Li, W.; Li, H.; Liu, Y.; Li, K.; Xie, K.; Li, X.; Fu, Q.; Cheng, L.; Zhang, L.; Wei, B. Carbon Nanotube-Multilayered Graphene Edge Plane Core-Shell Hybrid Foams for Ultrahigh-Performance Electromagnetic-Interference Shielding. *Adv. Mater.* **2017**, *29*, No. 1701583.
(22) Wang, Y.; Li, M.; Gu, Y.; Zhang, X.; Wang, S.; Li, Q.; Zhang, Z. Tuning Carbon Nanotube Assembly for Flexible, Strong and Conductive Films. *Nanoscale* **2015**, *7*, 3060−3066.
(23) Tang, H.; Hessel, C. M.; Wang, J.; Yang, N.; Yu, R.; Zhao, H.; Wang, D. Two-Dimensional Carbon Leading to New Photoconversion Processes. *Chem. Soc. Rev.* **2014**, *43*, 4281.
(24) Ma, M.; Tocci, G.; Michaelides, A.; Aeppli, G. Fast diffusion of water nanodroplets on graphene. *Nat. Mater.* **2016**, *15*, 66.
(25) Geim, A. K.; Grigorieva, I. V. Van der Waals heterostructures. *Nature* **2013**, *499*, 419.
(26) Novoselov, K. S.; Fal'ko, V. I.; Colombo, L.; Gellert, P. R.; Schwab, M. G.; Kim, K. A roadmap for graphene. *Nature* **2012**, *490*, 192.
(27) Hummers, W.; Offeman, R. J. Preparation of Graphitic Oxide. *J. Am. Chem. Soc.* **1958**, *80*, 1339−1340.
(28) Rodriguez-Navarro, C.; Suzuki, A.; Ruiz-Agudo, E. Alcohol Dispersions of Calcium Hydroxide Nanoparticles for Stone Conservation. *Langmuir* **2013**, *29*, 11457.
(29) Galan, I.; Glasser, F. P.; Baza, D.; Andrade, C. Assessment of the Protective Effect of Carbonation on Portlandite Crystals. *Cem. Concr. Res.* **2015**, *74*, 68.
(30) Pesce, G. L.; Fletcher, I. W.; Grant, J.; Molinari, M.; Parker, S. C.; Ball, R. J. Carbonation of Hydrous Materials at the Molecular Level: A Time of Flight-Secondary Ion Mass Spectrometry, Raman and Density Functional Theory Study. *Cryst. Growth Des.* **2017**, *17*, 1036.
(31) Ruiz-Agudo, E.; Kudlacz, K.; Putnis, C. V.; Putnis, A.; RodriguezNavarro, C. Dissolution and Carbonation of Portlandite [$Ca(OH)_2$] Single Crystals. *Environ. Sci. Technol.* **2013**, *47*, 11342.
(32) Natali, I.; Saladino, M. L.; Andriulo, F.; Chillura Martino, D.; Caponetti, E.; Carretti, E.; Dei, L. Consolidation and Protection by Nanolime: Recent Advances for the Conservation of the Graffiti, *Carceri dello Steri* Palermo and of the 18th Century Lunettes, SS. Giuda e Simone Cloister, Corniola (Empoli). *J. Cult. Heritage* **2014**, *15*, 151.


https://doi.org/10.1021/acsomega.2c01364
*ACS Omega* 2022, 7, 12424−12429